Magnetization switching behavior with competing anisotropies in epitaxial Co_3FeN/MnN exchange-coupled bilayers

T. Hajiri,[1,*] T. Yoshida,[1] S. Jaiswal,[2,3] M. Filianina,[2] B. Borie,[2,4] H. Ando,[1] H. Asano,[1] H. Zabel,[2] and M. Kläui[2]

[1]*Department of Crystalline Materials Science, Nagoya University, Nagoya 464-8603, Japan*

[2]*Institut für Physik, Johannes Gutenberg Universität, Staudingerweg 7, Mainz, D-55128, Germany*

[3]*Singulus Technologies AG, Kahl am Main, D-63796, Germany*

[4]*Sensitec GmbH, Hechtsheimer Strasse 2, Mainz, D-55131, Germany*

(Received 25 July 2016; revised manuscript received 6 October 2016; published 11 November 2016)

We report unusual magnetization switching processes and angular-dependent exchange bias effects in fully epitaxial Co_3FeN/MnN bilayers, where magnetocrystalline anisotropy and exchange coupling compete, probed by longitudinal and transverse magneto-optic Kerr effect (MOKE) magnetometry. The MOKE loops show multistep jumps corresponding to the nucleation and propagation of 90° domain walls in as-grown bilayers. By inducing exchange coupling, we confirm changes of the magnetization switching process due to the unidirectional anisotropy field of the exchange coupling. Taking into account the experimentally obtained values of the fourfold magnetocrystalline anisotropy, the unidirectional anisotropy field, the exchange-coupling constant, and the uniaxial anisotropy including its direction, the calculated angular-dependent exchange bias reproduces the experimental results. These results demonstrate the essential role of the competition between magnetocrystalline anisotropy and exchange coupling for understanding and tailoring exchange-coupling phenomena usable for engineering switching in fully epitaxial bilayers made of tailored materials.

DOI: 10.1103/PhysRevB.94.184412

I. INTRODUCTION

Thin epitaxial magnetic films are known to exhibit unusual magnetization switching processes resulting from competing anisotropies. Such unusual magnetization switching processes have frequently been observed due to the competition between fourfold magnetocrystalline anisotropy and additional uniaxial or unidirectional anisotropies resulting in multistep hysteresis loops [1–5]. The model adapted for explaining the unusual magnetization process has so far been based on total energy minimization and has assumed 90° domain wall nucleation and propagation [1,3]. Up to now, there have been several reports regarding unusual magnetization switching processes in systems where the magnetocrystalline anisotropy competes with an additional uniaxial anisotropy, such as an exchange-coupling-induced anisotropy [3,5–7], as well as uniaxial anisotropy induced by oblique growth [1,2]. Since uniaxial anisotropy induced by oblique growth is static and cannot be manipulated after growth, using exchange bias is a more exciting approach, which can be set and erased again even after film deposition and thus allows for tailoring and flexible manipulation of the switching. However, the effects of exchange coupling competing with magnetocrystalline anisotropies on the shape of the hysteresis loops have only been discussed for the case of Fe on IrMn and MnPd epitaxial bilayers [5,7,8]. The switching behavior of the epitaxial Co/CoO system has also been studied using anisotropic magnetoresistance [9] and x-ray magnetic circular/linear dichroism [10]. Only fully epitaxial stacks allow for maximum control of the properties, and using more advanced compounds has been suggested as these can exhibit a range of exciting properties [11], such as high spin polarization, which is needed for spintronics devices [12]. Thus, there is a clear need to study changes in magnetization switching processes due to the magnetocrystalline anisotropy and the exchange coupling in complex high-quality heterostructures with tailored properties.

A particularly exciting compound is the antiperovskite nitride Co_3FeN (CFN) as it is theoretically expected to be a half-metallic ferromagnet (FM) with a negative spin polarization [13]. Therefore, combining it with an antiferromagnet (AFM) as well as with a positive-spin-polarization FM [14] is of great promise for spintronic applications. CFN exhibits a fourfold magnetocrystalline anisotropy of 3.5×10^4 J/m^3 [15], which is smaller than for Fe (4.8×10^4 J/m^3) [16]. The antiperovskite nitride shows a multistep hysteresis without any uniaxial anisotropy [17], allowing us to compare the change in magnetization switching processes in the presence or absence of an exchange coupling. The θ phase of MnN is a collinear I-type antiferromagnet with a high Néel temperature of 640 K [18], where the spins align parallel within the *ab* plane and alternate along the *c*-axis direction. Since MnN does not contain rare metals but nevertheless exhibits a high Néel temperature, MnN is considered to replace typical AFMs such as IrMn and PtMn [19]. In fact, large exchange bias has been reported in MnN/CoFe polycrystalline bilayers even at room temperature [19].

Exchange coupling at the interfaces between FM and AFM has been widely studied because of the general interest in spintronic devices such as spin-valve-type magnetic memory devices [20,21]. In addition, since AFM magnetic moments can be controlled and detected via exchange coupling, this approach has recently attracted much attention [22,23]. In particular, the possibility of current-induced magnetization switching of AFM spins was reported in CFN/Mn_3GaN epitaxial bilayers [23]. Since the Néel temperature of Mn_3GaN is low (∼280 K), similar studies using an AFM with a much higher Néel temperature such as MnN are desired. Revealing the magnetic properties of fully epitaxial CFN/MnN bilayers is therefore an important step to generate novel

*t.hajiri@numse.nagoya-u.ac.jp

spintronic devices using exchange coupling with a negative-spin-polarized half-metallic FM at room temperature, which is a key motivation for such studies. The principal features of the exchange coupling such as the shift of hysteresis loops (exchange bias) and the broadening of the coercivity are well known [24,25], and the angular-dependent exchange bias model has been well defined and performed for polycrystalline bilayers [24,26,27]. However, there are few studies of fully epitaxial bilayers [28,29], and in these studies anisotropies have been small or neglected; thus, this additional degree of freedom for tuning the switching has not been discussed. On the other hand, systematic theoretical studies of the competition between different anisotropies have been carried out [30,31]. Therefore, to understand the interplay between intrinsic static magnetocrystalline anisotropies and tunable exchange bias leading to tailored switching, an in-depth study of a fully epitaxial stack with both significant anisotropies and exchange bias is needed.

In this work, we perform longitudinal and transverse magneto-optic Kerr effect (MOKE) magnetometry measurements to determine the magnetization switching process and the angular-dependent exchange bias in fully epitaxial CFN/MnN bilayers, where the magnetocrystalline anisotropy and an exchange coupling compete. Multistep MOKE loops were observed that corresponded to the magnetization switching between the different fourfold-symmetry easy axes. Comparing as-grown bilayers and those with field cooling (FC), we explore the change in the magnetization switching process around the direction perpendicular to FC. By a numerical analysis based on the Stoner-Wohlfarth model using experimentally determined magnetocrystalline anisotropy and exchange-coupling terms, we determine the angular-dependent exchange bias that qualitatively reproduces the experimental results. These results could provide a route to understanding exchange-coupling phenomena of fully epitaxial bilayers when the competition between the magnetocrystalline anisotropy and an additional uniaxial anisotropy yields unusual magnetization switching processes.

II. EXPERIMENTAL DETAILS

High-quality epitaxial CFN (5 nm)/MnN (30 nm) bilayers with a Hf capping layer (3 nm) were fabricated by reactive magnetron sputtering on $MgAl_2O_4$ substrates. MnN and CFN were grown at 450 °C and 350 °C substrate temperatures, using 40% N_2 + 60% Ar and 15% N_2 + 85% Ar gas mixtures, respectively. The lattice mismatch is 11.8% between CFN and MnN and 3.5% between MnN and $MgAl_2O_4$ substrates. After bilayer growth, we obtained the exchange bias by annealing at 400 °C for 30 min while applying a field of 200 mT at a base pressure of 3.0×10^{-6} Pa and then cooling to room temperature while applying a field of 200 mT. The applied field was along the easy axis ⟨110⟩ of CFN. The crystal structure was analyzed using both in-plane and out-of-plane x-ray diffraction (XRD) measurements with Cu $K\alpha$ radiation. The magnetic properties were characterized by vibrating sample magnetometry and the magneto-optic Kerr effect in longitudinal and transverse geometry, called Lo-MOKE and Tr-MOKE, respectively. For MOKE magnetometry measurements, we used two setups. Angular-dependent Lo-MOKE measurements were performed using a red (635-nm) low-noise laser diode. The comparison between Lo- and Tr-MOKE magnetometries was performed by Kerr microscopy. Both MOKE magnetometry measurement types were performed at room temperature.

III. RESULTS AND DISCUSSION

The XRD patterns of CFN/MnN bilayers are shown in Figs. 1(a) and 1(b). As shown in Fig. 1(a), only the (00l) CFN and (l00) MnN peak series exhibit Bragg peaks in the out-of-plane XRD, which indicates that (001)-oriented CFN grows on (100)-oriented MnN. In addition, the epitaxial growth is confirmed by the results of the ϕ-scan measurement, as shown in Fig. 1(b), indicating that their epitaxial relationship is CFN(001)[100]//MnN(100)[001]//$MgAl_2O_4$(001)[100]. The magnetic properties of the as-grown CFN/MnN bilayers are shown in Figs. 1(c) and 1(d). The angular dependence of the ratio of the remanent and saturation magnetization M_r/M_s of as-grown CFN/MnN bilayers is shown in Fig. 1(c). The as-grown CFN/MnN bilayers exhibit clear fourfold magnetocrystalline anisotropy with the easy axis oriented along the CFN⟨110⟩ crystalline directions and the hard axis oriented along the CFN⟨100⟩ crystalline directions, which is consistent with the case of only a single-layer CFN film [15]. The hysteresis loop along the hard axis of the CFN/MnN bilayers is shown in Fig. 1(d). To determine the magnitude of the two- and fourfold magnetocrystalline anisotropy constants K_u and K_1 of the CFN/MnN bilayers, we applied the Stoner-Wohlfarth model [32] to fit the reversible part of the obtained hysteresis loop along the hard-axis of the CFN/MnN bilayers in the same manner as done before with only CFN thin films [15]. As shown in Fig. 1(d), the Stoner-Wohlfarth model allows us to reproduce the reversible part of the hysteresis loop assuming a fourfold magnetocrystalline anisotropy constant K_1 of $33\,700 \pm 250$ J/m^3, without any uniaxial anisotropy contribution. The estimated value of K_1 is comparable with that of only CFN ($K_1 = 34\,850 \pm 250$ J/m^3) [15]. We should note that the exchange coupling might exist even in as-grown bilayers [33,34]. Actually, some angles show small hysteresis shifts (up to 1 mT), while most angles show almost zero hysteresis shift (less than 0.2 mT), which is shown below in Fig. 6(a). Since small hysteresis shifts seem to be random and there is almost zero hysteresis shift of Fig. 1(d), we consider only the CFN magnetocrystalline anisotropy and ignore the contribution from any further exchange coupling.

Next, we turn our attention to the in-plane angular-dependent Lo-MOKE loops. The Lo-MOKE loops were measured between 0° and 360° in steps of 5°. The normal MOKE loops are observed around the fourfold easy ($\theta = 45°$, 135°) and hard axes ($\theta = 0°$, 90°, 180°) in the case of as-grown bilayers, as shown in Fig. 2(a). Multistep MOKE loops are visible when the field is applied along an axis between the easy and hard axes (for example, $\theta = 10°$–30°). The multistep MOKE loops are present with a 45° periodicity, reflecting the fourfold magnetocrystalline anisotropy. In the case with FC as shown in Fig. 2(b), however, the fourfold crystalline symmetry is broken along the direction perpendicular to FC ($\theta = 135°$). Although normal MOKE loops with shifts due to exchange bias are observed along easy axis $E1$, which is parallel to

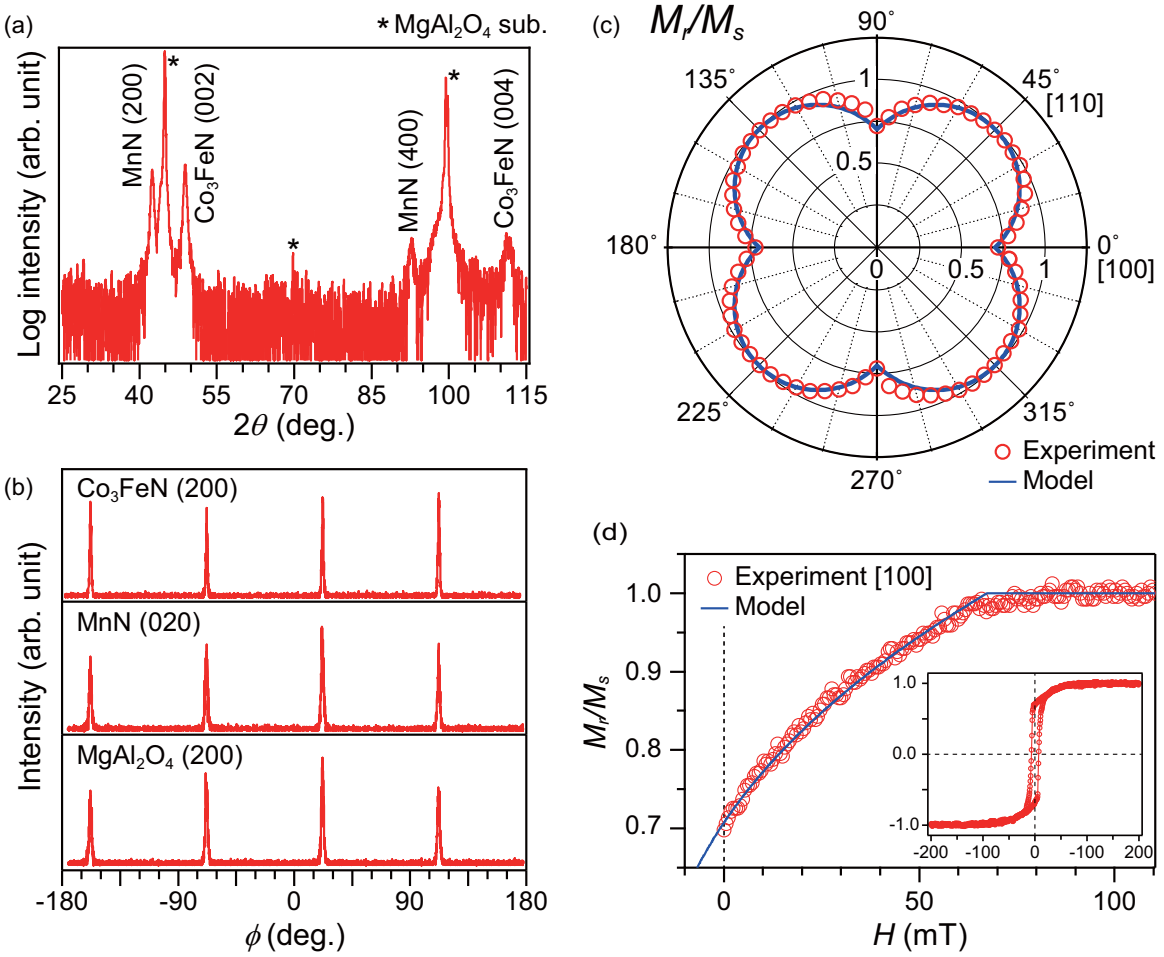

FIG. 1. (a) Out-of-plane and (b) in-plane ϕ scans of CFN/MnN bilayers. (c) Angular dependence of M_r/M_s of as-grown CFN/MnN bilayers. The solid line is estimated from the Stoner-Wohlfarth model using $K_1 = 33\,700\ \mathrm{J/m^3}$. (d) Comparison of the magnetic hysteresis loop reversible part along the hard axis [100] with the model. The inset shows the magnetic hysteresis loop along the hard axis [100].

FC ($\theta = 45°$), and hard axes ($\theta = 0°$, $90°$, $180°$), the other easy axis, $E2$, which is perpendicular to the FC direction ($\theta = 135°$), shows multistep hysteresis. The multistep height changes continuously from $90°$ to $180°$.

In order to compare the magnetization switching process in the presence and absence of FC, we performed Tr-MOKE magnetometry measurements as well as Lo-MOKE magnetometry measurements. In both cases, the multistep Lo-MOKE loops are clearly observed, and these steps show good agreement with Tr-MOKE loops, as shown in Fig. 3. In the case of as-grown bilayers, the convexities change during the field sweep in Tr-MOKE loops; for example, at $\theta = 100, 110°$, upward and downward convexities [see Fig. 3(a), $100°$ green arrows] are present during positive to negative and negative to positive field sweeps, respectively. At $\theta = 135°$, there is no Tr-MOKE signal. At $\theta = 150°$, $160°$, $170°$, the convexities are reversed compared to the orientations from $\theta = 100°$, $110°$; downward and upward convexities are present during positive to negative and negative to positive field sweeps, respectively. In the case with FC, the same convexities are exhibited at $\theta = 100°$, $170°$. On the other hand, at $\theta = 120°$, $135°$, $150°$, only the downward convexities are exhibited during both field sweeps.

According to the $90°$ domain wall nucleation and propagation model, the multistep positions correspond to the magnetization switching between two easy axes of the fourfold anisotropy [1,4]. These $90°$ switching fields are expressed by following equations [1,4]:

$$
\begin{aligned}
H_{E1\to E2} &= \frac{E_{1\to 2} + E_{eb} + K_{u,eb}}{M_s(\sin\phi - \cos\phi)},\\
H_{E1\to E4} &= \frac{E_{1\to 4} + E_{eb} + K_{u,eb}}{M_s(-\sin\phi - \cos\phi)},\\
H_{E2\to E3} &= \frac{E_{2\to 3} + E_{eb} - K_{u,eb}}{M_s(-\sin\phi - \cos\phi)},\\
H_{E4\to E3} &= \frac{E_{4\to 3} + E_{eb} - K_{u,eb}}{M_s(\sin\phi - \cos\phi)},\\
H_{E3\to E4} &= \frac{E_{3\to 4} - E_{eb} + K_{u,eb}}{M_s(-\sin\phi + \cos\phi)},\\
H_{E3\to E2} &= \frac{E_{3\to 2} - E_{eb} + K_{u,eb}}{M_s(\sin\phi + \cos\phi)},\\
H_{E4\to E1} &= \frac{E_{4\to 1} - E_{eb} - K_{u,eb}}{M_s(\sin\phi + \cos\phi)},\\
H_{E2\to E1} &= \frac{E_{2\to 1} - E_{eb} - K_{u,eb}}{M_s(-\sin\phi + \cos\phi)},
\end{aligned}
\qquad (1)
$$

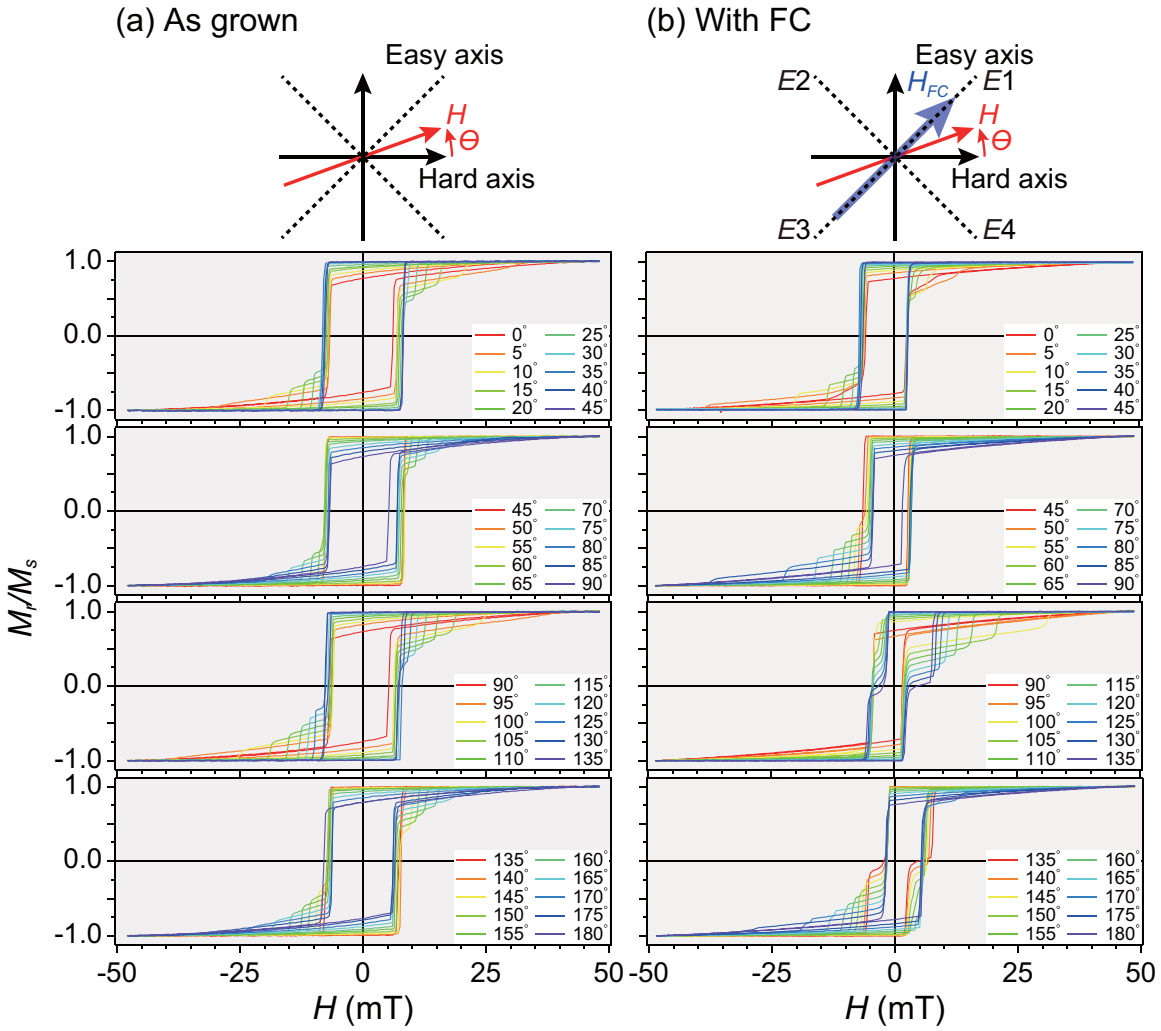

FIG. 2. Series of angular-dependent Lo-MOKE loops (a) in the as-grown case and (b) with FC. The top panels show the experimental configuration.

where $H_{E1\to E2}$ and $E_{1\to 2}$ are the switching field and the domain wall nucleation energy from easy axis $E1$ to easy axis $E2$ as assigned in the top panel of Fig. 2(b), respectively, E_{eb} is the unidirectional anisotropy due to exchange coupling, $K_{u,ex}$ is the uniaxial anisotropy along the FC direction, M_s is the saturation magnetization, and ϕ is the applied field orientation from the easy axis $E1$ ($\phi = \theta + 45$, θ is defined in Fig. 2). The step positions (open circles) and model fitting results using Eq. (1) (solid lines) in both the presence and absence of FC are shown in Fig. 4. In the case of as-grown bilayers shown in Fig. 4(a), the additional step positions exhibit a clear fourfold symmetry, reflecting the magnetocrystalline anisotropy. The additional step positions are reproduced by Eq. (1), without any exchange-coupling contributions, whereas the main step positions corresponding to the coercive field H_c are not reproduced well. In the case with FC, on the other hand, angular-dependent step positions do not exhibit fourfold symmetry, indicating the broken symmetry of fourfold magnetocrystalline anisotropy, as mentioned above. Taking into account the exchange-coupling contributions, all step positions can be reproduced well. Comparing the presence and absence of FC, the magnetization switching processes are the same at $\theta = 0°$–$90°$ and $180°$–$270°$ except for the lack of the $E2\to E1$ jump that occurs with FC. At $\theta = 90°$–$180°$ and $270°$–$360°$, the magnetization switching processes are not the same, and these results are consistent with the change of convexity in the Tr-MOKE loops, as shown in Fig. 3.

In Fig. 5 we summarize the change in the magnetization switching process, as well as show the Lo- and Tr-MOKE loops around the direction perpendicular to FC (at $\theta = 110°$ for the case of as-grown bilayers and at $\theta = 120°$ for the case with FC). As already shown in Fig. 3, the Tr-MOKE loop at $\theta = 110°$ of as-grown bilayers shows the upward and the downward convexities between field sweeps in Fig. 5(a). When the field is swept from positive to negative (from negative to positive), the magnetization switching follows the following process, as shown in Fig. 5(b) [Fig. 5(c)]:

(i) The saturation magnetization follows the applied field direction.

(ii) The magnetization rotates towards the nearest easy axis $E2$ ($E4$) continuously without a jump in the MOKE loop.

(iii) The magnetization jumps in a direction close to the other easy axis $E3$ ($E1$) from $E2$ ($E4$).

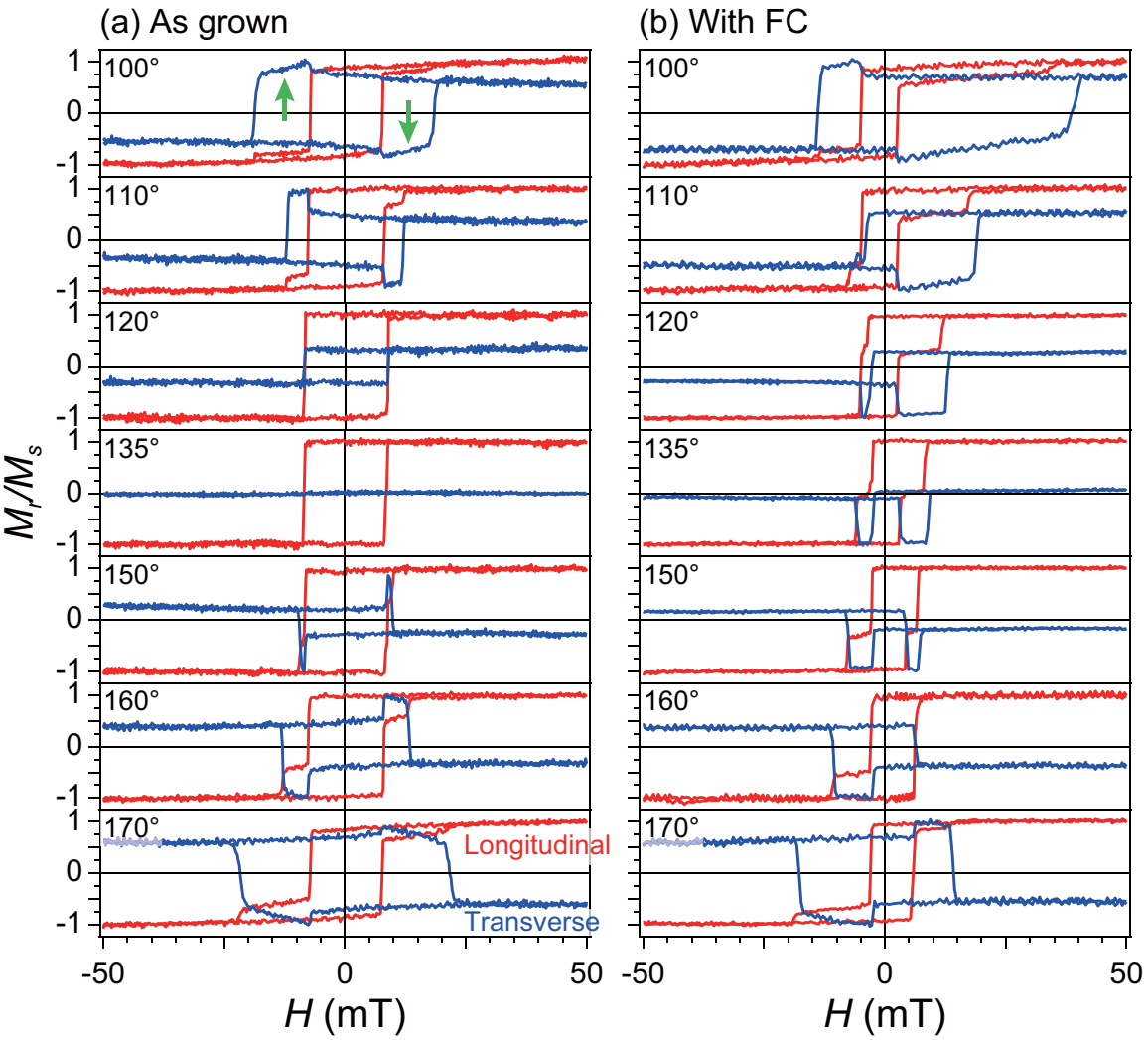

FIG. 3. Comparison between Lo- and Tr-MOKE loops (a) in the as-grown case and (b) with FC around the direction perpendicular to FC. Measurement angles are the same as those in Fig. 2. The arrows at 100° in (a) indicate upward and downward convexities of the Tr-MOKE loop.

(iv) The magnetization jumps to a position close to the other easy axis but along the opposite direction $E4$ ($E2$) from $E3$ ($E1$).

(v) The magnetization finally rotates towards the applied field direction without a jump in the MOKE loop.

The magnetization switching process follows different paths for sweeping the field up or down in the case of as-grown bilayers. On the other hand, the Tr-MOKE loop with FC shows only downward convexities between both field sweeps in Fig. 5(d), showing a qualitatively different behavior. The magnetization switching processes are similar to those in the case of as-grown bilayers, but the magnetization switching processes follow the same path between both field sweeps, as shown in Fig. 5(e) and 5(f). These results indicate that the magnetization switching via $E1$ is energetically favored over magnetization switching via $E3$ around the direction perpendicular to FC due to the unidirectional anisotropy field resulting from the interfacial uncompensated spins aligned along $E1$ [3,5]. It is noted that the same feature appears around $\theta = 315°$. In case of the uniaxial anisotropy induced by oblique growth, $E1$ and $E3$ are energetically equivalent, so that the change in the magnetization switching process does not occur [1,2], showing a clear difference from the observed behavior here. This fact demonstrates the impact of an exchange bias that governs the magnetization switching process.

After clarifying the magnetization switching process of fully epitaxial CFN/MnN exchange-coupled bilayers, we finally turn our attention to their angular-dependent exchange bias. Figure 6(a) shows the angular-dependent exchange bias of CFN/MnN exchange-coupled bilayers obtained from Lo-MOKE loops. The exchange bias shows some steps occurring approximately every 45°. Then, the exchange bias shows an abrupt sign change in the direction perpendicular to the FC ($\theta = 135$ and 315°). For the polycrystalline exchange-coupled bilayers, the angular-dependent exchange bias shows the maximum along the FC direction and gradually decreases towards the direction perpendicular to FC. It then changes its sign continuously after the direction perpendicular to FC [24,26,27]. Since there is no magnetocrystalline anisotropy in polycrystalline bilayers, the observed angular-dependent exchange bias is considered to highlight the importance of the

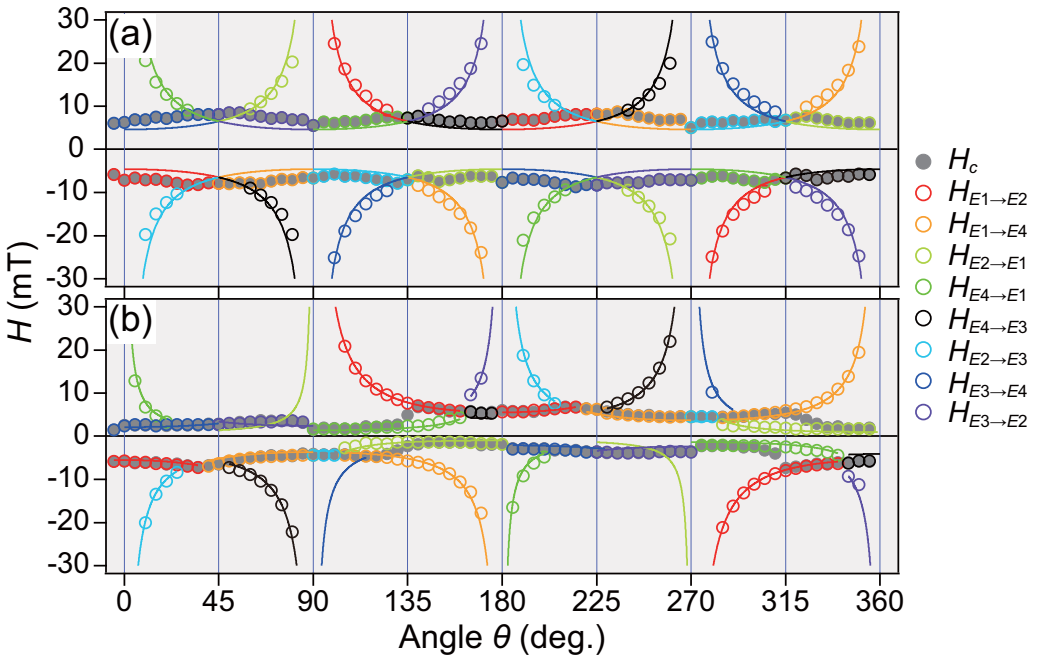

FIG. 4. The angular-dependent step positions as a function of angle (a) in the as-grown case and (b) with FC. The open circles and solid lines are experimental data and model fittings, respectively.

competition between magnetocrystalline anisotropy and the uniaxial anisotropy due to exchange coupling. In fact, recent theoretical studies based on a Stoner-Wohlfarth model, which discussed the effect of fourfold anisotropy, predict a similar angular dependence [30,31].

According to recent theoretical studies, the free energy of the exchange-coupled bilayer can be expressed as

$$E = -M_s H t_F \cos\theta + t_F K_{u,ex} \sin^2(\theta - \theta_{u,ex}) + t_F K_1 \sin^2(\theta - \theta_c)\cos^2(\theta - \theta_c) - J_E \cos(\theta - \theta_{FC}), \quad (2)$$

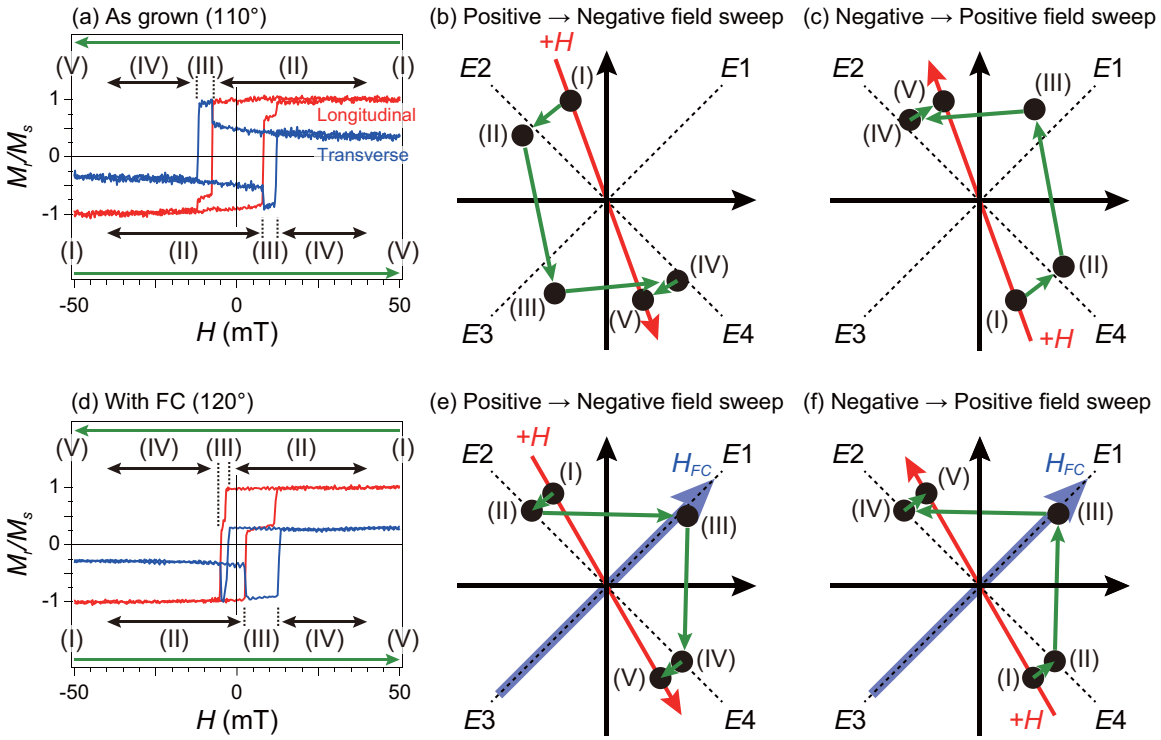

FIG. 5. Comparison of the magnetization switching process between (a)–(c) the as-grown case and (d)–(f) the case with FC. (a), (d) Lo- and Tr-MOKE loops. The schematic magnetization switching process is shown for (b) and (e) positive to negative and (c) and (f) negative to positive field sweeps.

where θ is the magnetization angle from the applied field direction; $\theta_{u,ex}$, θ_c, and θ_{FC} are the angles between the uniaxial anisotropy and applied field direction, between the fourfold magnetocrystalline anisotropy and applied field direction, and between the FC and applied field direction, respectively; and J_E is the exchange-coupling constant [30,31]. The uniaxial anisotropy can be caused by noncollinear FC or interfacial frustration [35,36]. The direction of uniaxial anisotropy depends on the ratio between FM anisotropy and AFM anisotropy, and its direction is from the FC direction to the direction perpendicular to the FC [35]. To determine the uniaxial anisotropy direction, we calculate the Tr-MOKE loops for three different configurations (the angles between uniaxial anisotropy and the FC direction $\theta_{u,ex} - \theta_{FC} = 0^\circ, 45^\circ, 90^\circ$), as shown in Fig. 6(b). Here, we use the anisotropy constants determined from the switching position fitting, as shown in Fig. 4(b). When the uniaxial anisotropy is parallel to the FC direction, since the ratio $E_{1\to2} : E_{eb} : K_{u,ex}$ is obtained as 7.5 : 3.5 : 1 from the fitting results of Fig. 4 and $E_{1\to2}$ and E_{eb} can replace K_1 and J_E/t_F, respectively [5], J_E/t_F and $K_{u,ex}$ can be determined from the K_1 value as ∼16 and ∼5 kJ/m^3, respectively. When the uniaxial anisotropy is perpendicular to FC, the signs of $K_{u,ex}$ terms in Eq. (1) are reversed. Then, in the same manner, J_E/t_F and $K_{u,ex}$ can be determined from the K_1 value as ∼14 and ∼4.3 kJ/m^3, respectively. On the other hand, when the uniaxial anisotropy is 45° from the FC direction, we cannot determine the uniaxial anisotropy constant from the switching positions because there is no or a much smaller contribution to the magnetization switching position in the 90° domain wall nucleation and propagation model. Therefore, we use the anisotropy constants in the case of the parallel-to-FC configuration in Fig. 4(b). Although the magnetization switching processes at 135° are the same between the three different configurations as shown in Fig. 6(b), the switching behaviors of the other angles are quite different. Compared with the experimental Tr-MOKE loops shown in Fig. 3(b), the $\theta_{u,ex} - \theta_{FC} = 90^\circ$ configuration shows better agreement with experimental Tr-MOKE loops than the $\theta_{u,ex} - \theta_{FC} = 0^\circ$ and 45° configurations. This fact might indicate that the MnN anisotropy is much larger than CFN [35]. The same 90° configuration was observed in Fe/FeF$_2$ epitaxial bilayers [37]. Recent theoretical studies take into account the uniaxial anisotropy but consider only a fixed configuration [30,31]. Our results imply the importance of the uniaxial anisotropy direction induced by noncollinear FC or interfacial frustration [35,36].

The calculated angular-dependent exchange bias for $\theta_{u,ex} =$ 90° is shown in Fig. 6(a), along with the experimental result. The calculations reproduce the experimental results well, except for the angles between 0° and 45° and between 180° and 225°. One possible cause of this inconsistency for the angles between 0° and 45° and between 180° and 225° are the different magnetization switching processes. Comparing the calculated hysteresis loops with experimental Lo- and Tr-MOKE loops, as shown in Fig. 7(a), the multistep hysteresis loops at $\theta = 60^\circ$ and 135° are qualitatively well reproduced by the presented model. At $\theta = 15^\circ$, however, although the experimental Lo- and Tr-MOKE loops show the multistep on both the positive and negative field sides, the calculated loops show the multistep only on the negative

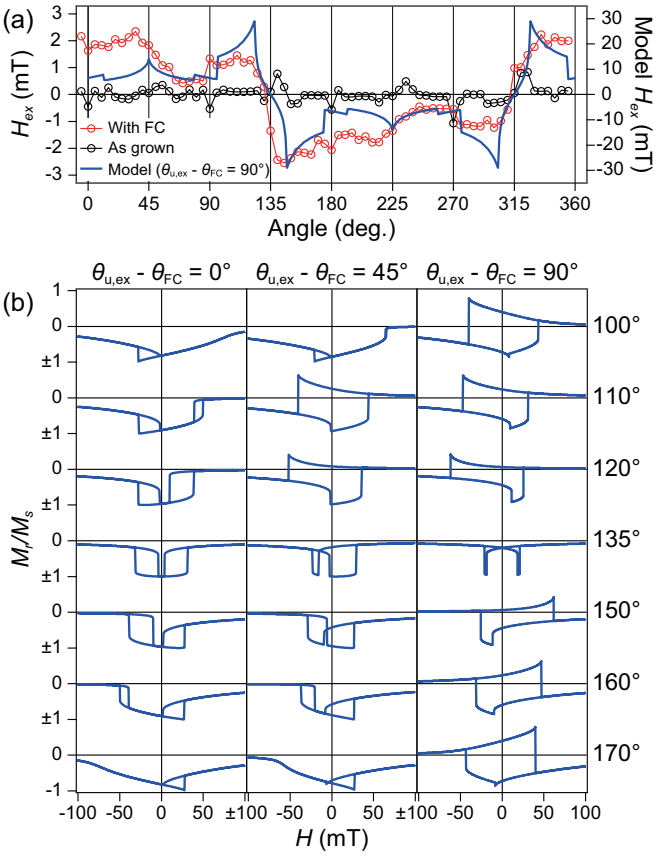

FIG. 6. (a) Comparison of angular-dependent exchange bias H_{ex} with the model using $K_1 = 33\,700$ J/m^3, $J_E = 14\,000$ J/m^3, $K_{u,ex} = 4300$ J/m^3, and $\theta_{u,ex} = 90^\circ$. (b) $\theta_{u,ex}$-dependent calculated Tr-MOKE loops of various applied field angles around the direction perpendicular to FC using $K_1 = 33\,700$ J/m^3, $J_E = 16\,000$ J/m^3, and $K_{u,ex} = 5000$ J/m^3 for $\theta_{u,ex} = 0^\circ$ and 45° and $K_1 = 33\,700$ J/m^3, $J_E = 14\,000$ J/m^3, and $K_{u,ex} = 4300$ J/m^3 for $\theta_{u,ex} = 90^\circ$.

field side, indicating that the magnetization switching process is different. These results indicate that we succeeded in determining the magnetocrystalline anisotropy and the exchange-coupling terms with the 90° domain wall nucleation and propagation model to reproduce the angular-dependent exchange bias as well as hysteresis loops, but we should take into account other complex anisotropies due to spin disorder at the FM/AFM interface, AFM anisotropy, and/or rotatable interfacial uncompensated spins [24,27]. The other possible cause is the domain nucleation. Since the Stoner-Wohlfarth model is a single-domain model designed for describing magnetization switching in magnetic nanoparticles, a Stoner-Wohlfarth model cannot describe the domain nucleation. Actually, we observe such a 90° domain nucleation exhibiting a multistep in the Kerr measurements, as shown in Fig. 7(b). The Kerr microscopy imaging shows spins aligned along the $E2$ direction (single domain) at the positive saturated field. In the first step ($H \sim -2.7$ mT), the 90° domain nucleates where the spins align along the $E1$ direction. Then, the 90° domain propagates between two steps ($H \sim -5.3$ mT). In the second step ($H \sim -5.8$ mT), the 90° domain nucleates where the spins align along the $E4$ direction. Finally, the 90° domain

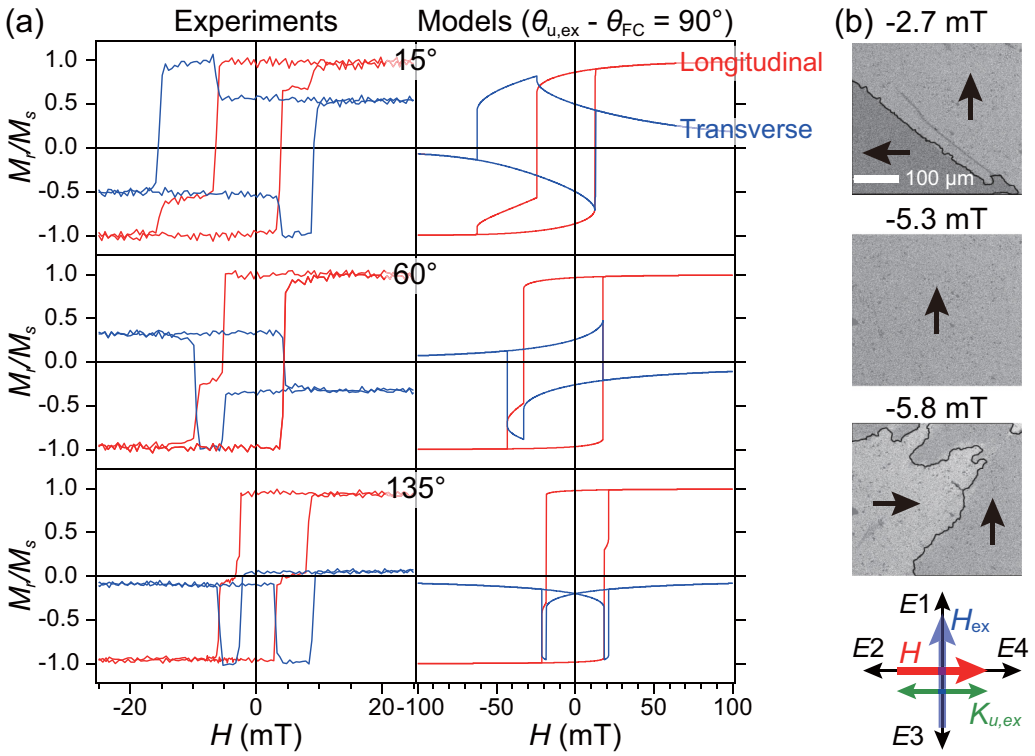

FIG. 7. (a) Comparison of experimental and calculated Lo- and Tr-MOKE loops. Experimental results are normalized by maximum/minimum signals. (b) Domain structures during positive to negative field sweep at $\theta = 135°$ obtained at the Lo-MOKE setup, where arrows indicate the relative orientations of the magnetization.

wall propagates and becomes a single domain. While domain nucleation can explain some of the discrepancies between model calculations and experiment, our model calculation of the angular dependence of exchange bias reproduces a trend similar to that in the experimental results for a large range of angles, showing that coherent rotation dominates in this range. Therefore, our results demonstrate that the interplay between the magnetocrystalline anisotropy and the additional uniaxial anisotropies plays an important role in the angular-dependent exchange bias as well as the magnetization switching process.

IV. CONCLUSION

We performed Lo- and Tr-MOKE magnetometry measurements that allowed us to clarify the magnetization switching process and the angular-dependent exchange bias of fully epitaxial CFN/MnN bilayers, where the fourfold magnetocrystalline anisotropy and the tunable unidirectional anisotropy due to exchange coupling compete. The magnetization switching process of these bilayers can be reproduced by combining a Stoner-Wohlfarth model and a 90° domain wall nucleation and propagation model. We found a major qualitative difference in the magnetization switching processes in the presence or absence of FC, indicating the influence of the tunable exchange coupling competing with the growth-induced magnetocrystalline anisotropy. By performing a numerical analysis taking into account the experimentally determined magnetocrystalline anisotropy and exchange-coupling terms, we clarified the direction of the uniaxial anisotropy caused by noncollinear FC or interfacial frustration along a direction perpendicular to the FC. Finally, we calculated the angular dependence of the exchange bias, reproducing the experimental results for a large range of angles. These results provide profound insight into exchange-coupling phenomena in fully epitaxial bilayers and a guide to potential applications in the field of spintronics using advanced materials with possible half-metallicity combined with exchange coupling.

ACKNOWLEDGMENTS

The authors gratefully acknowledge D. Oshima, T. Kato, and S. Iwata for their assistance with annealing and FC processes. This work was supported by the Japan Society for the Promotion of Science (JSPS) Program for Advancing Strategic International Networks to Accelerate the Circulation of Talented Researchers, the Center for Spintronics Research Network (CSRN), Tohoku University, the Deutsche Forschungsgemeinschaft (DFG, SFB TRR 173 Spin+X in particular the visiting guest researcher program), and the Graduate School of Excellence Materials Science in Mainz (GSC 266). S.J., B.B., and M.K. gratefully acknowledge the European Union for funding under the FP7 Marie Curie ITN WALL project/Grant No. FP7-PEOPLE-2013-ITN 608031.

[1] R. P. Cowburn, S. J. Gray, and J. A. C. Bland, Phys. Rev. Lett. **79**, 4018 (1997).

[2] R. P. Cowburn, S. J. Gray, J. Ferré, J. A. C. Bland, and J. Miltat, J. Appl. Phys. **78**, 7210 (1995).

[3] E. Arenholz and K. Liu, Appl. Phys. Lett. **87**, 132501 (2005).
[4] Y. Zhang, Q. Zhan, Z. Zuo, H. Yang, X. Zhang, G. Dai, Y. Liu, Y. Yu, J. Wang, B. Wang, and R.-W. Li, Phys. Rev. B **91**, 174411 (2015).
[5] W. Zhang, M. E. Bowden, and K. M. Krishnan, Appl. Phys. Lett. **98**, 092503 (2011).
[6] W. Zhang and K. M. Krishnan, J. Magn. Magn. Mater. **324**, 3129 (2012).
[7] Q. F. Zhan and K. M. Krishnan, J. Appl. Phys. **107**, 09D703 (2010).
[8] Q. F. Zhan, W. Zhang, and K. M. Krishnan, Phys. Rev. B **83**, 094404 (2011).
[9] H.-L. Liu, S. Brems, Y.-J. Zeng, K. Temst, A. Vantomme, and C. V. Haesendonck, J. Phys. Condens. Matter **28**, 196002 (2016).
[10] R. Abrudan, J. Miguel, M. Bernien, C. Tieg, M. Piantek, J. Kirschner, and W. Kuch, Phys. Rev. B **77**, 014411 (2008).
[11] W. Zhanga and K. M. Krishnan, Mater. Sci. Eng. R **105**, 1 (2016).
[12] M. Jourdan, J. Minár, J. Braun, A. Kronenberg, S. Chadov, B. Balke, A. Gloskovskii, M. Kolbe, H. J. Elmers, G. Schönhense, H. Ebert, C. Felser, and M. Kläui, Nat. Commun. **5**, 3974 (2014).
[13] Y. Takahashi, Y. Imai, and T. Kumagai, J. Magn. Magn. Mater. **323**, 2941 (2011).
[14] T. Gushi, K. Ito, S. Honda, Y. Yasutomi, K. Toko, H. Oosato, Y. Sugimoto, K. Asakawa, N. Ota, and T. Suemasu, Jpn. J. Appl. Phys. **54**, 028003 (2015).
[15] T. Hajiri, S. Finizio, M. Vafaee, Y. Kuroki, H. Ando, H. Sakakibara, A. Kleibert, L. Howald, F. Kronast, K. Ueda, H. Asano, and M. Kläui, J. Appl. Phys. **119**, 183901 (2016).
[16] C. D. Graham, Phys. Rev. **112**, 1117 (1958).
[17] J. L. Costa-Krämer, D. M. Borsa, J. M. García-Martín, M. S. Martín-González, D. O. Boerma, and F. Briones, Phys. Rev. B **69**, 144402 (2004).
[18] K. Suzuki, T. Kaneko, H. Yoshida, Y. Obi, H. Fujimori, and H. Morita, J. Alloys Compd. **306**, 66 (2000).
[19] M. Meinert, B. Büker, D. Graulich, and M. Dunz, Phys. Rev. B **92**, 144408 (2015).
[20] S. A. Wolf, D. D. Awschalom, R. A. Buhrman, J. M. Daughton, S. von Molnár, M. L. Roukes, A. Y. Chtchelkanova, and D. M. Treger, Science **294**, 1488 (2001).
[21] J. Åkerman, Science **308**, 508 (2005).
[22] B. G. Park, J. Wunderlich, X. Martí, V. Holý, Y. Kurosaki, M. Yamada, H. Yamamoto, A. Nishide, J. Hayakawa, H. Takahashi, A. B. Shick, and T. Jungwirth, Nat. Mater. **10**, 347 (2011).
[23] H. Sakakibara, H. Ando, Y. Kuroki, S. Kawai, K. Ueda, and H. Asano, J. Appl. Phys. **117**, 17D725 (2015).
[24] F. Radu and H. Zabel, *Magnetic Heterostructures*, Springer Tracts in Modern Physics, Vol. 227 (Springer, Berlin, 2008), pp. 97–184.
[25] J. Nogués and I. K. Schuller, J. Magn. Magn. Mater. **192**, 203 (1999).
[26] J. Camarero, J. Sort, A. Hoffmann, J. M. García-Martín, B. Dieny, R. Miranda, and J. Nogués, Phys. Rev. Lett. **95**, 057204 (2005).
[27] F. Radu, A. Westphalen, K. Theis-Bröhl, and H. Zabel, J. Phys. Condens. Matter **18**, L29 (2006).
[28] D. Y. Kim, C. G. Kim, C.-O. Kim, M. Shibata, M. Tsunoda, and M. Takahashi, IEEE Trans. Magn. **41**, 2712 (2005).
[29] S. Dubourg, J. F. Bobo, B. Warot, E. Snoeck, and J. C. Ousset, Eur. Phys. J. B **45**, 175 (2005).
[30] Y. Bai and X. Xu, IEEE Trans. Magn. **51**, 4800404 (2015).
[31] A. E. Tillmanns and T. Blachowicz, J. Appl. Phys. **109**, 083923 (2011).
[32] E. C. Stoner and E. P. Wohlfarth, Philos. Trans. R. Soc. London, Ser. A **240**, 599 (1948).
[33] S. Anandakumar, V. S. Rani, S. Oh, and C. Kim, Thin Solid Films **519**, 1020 (2010).
[34] S. Brück, J. Sort, V. Baltz, S. Suriñach, J. S. Muñoz, B. Dieny, M. D. Baró, and J. Nogués, Adv. Mater. **17**, 2978 (2005).
[35] E. Jiménez, J. Camarero, J. Sort, J. Nogués, N. Mikuszeit, J. M. García-Martín, A. Hoffmann, B. Dieny, and R. Miranda, Phys. Rev. B **80**, 014415 (2009).
[36] E. Jiménez, J. Camarero, J. Sort, J. Nogués, A. Hoffmann, F. J. Teran, P. Perna, J. M. García-Martín, B. Dieny, and R. Miranda, Appl. Phys. Lett. **95**, 122508 (2009).
[37] T. J. Moran, J. Nogués, D. Lederman, and I. K. Schuller, Appl. Phys. Lett. **72**, 617 (1998).